REFERENCES

Abuluwefa, H.T., Guthrie, R.I.L. and Ajersch, F., 1996, *The effect of oxygen concentration on the oxidation of low- carbon steel in the temperature range 1000 to 1250°C,* Oxidation of Metals, **46**, 423 - 440

Abuluwefa, H.T., Guthrie, R.I.L. and Ajersch, F., 1997, *Oxidation of low carbon steel in multi-component gases: Part 1. Reaction mechanisms during isothermal oxidation*, Metallurgical and Materials Transactions series A, **28**, A, 1633 - 1641

Abuluwefa, H.T., Guthrie, R.I.L. and Ajersch, F., 1997, *Oxidation of low carbon steel in multi-component gases: Part 2. Reaction mechanisms during reheating*, Metallurgical and Materials Transactions series A, **28**, A, 1643 - 1651

Ajersch, F., 1992, *Scale formation in steel processing operations*, Mechanical working &steel processing conference, **30**, 419-437

Akiyama, T., Ohta, H., Takahashi, R., Waseda, Y. and Yagi, J., 1992, *Measurement and modeling of thermal conductivity for dense iron oxide and porous iron ore agglomerates in stepwise reduction.* ISIJ International, **32**, 829 - 837

Asai, T., Soshiroda, T. and Miyaharea, M., 1997, *Influence of Ni impurity in steel on the removability of primary scale in hydraulic descaling*, ISIJ International, **37**, 272 - 277

Blazevic, D.T., 1987, *Rolled in scale - the consistent problem*, 4th International Steel rolling conference, **1**. Deauville, France, 1-3 June 1987, A38.1 - A38.13

Boggs, W.E., 1973, *The role of structural and compositional factors in the oxidation of iron and iron-based alloys in high temperature gas-metal reactions in mixed environments*, Metallurgical society of AIME, 84 - 128

Boggs, W.E., Sonon, D.E., 1978, *Method for improving the surface quality of stainless steels and other chromium-bearing iron alloys.*, United States Patent 4078949

Douglass, D.L., 1995, *A critique of internal oxidation in alloys during the post-Wagner era.* Oxidation of Metals, **44**, 81 - 111

Engell, H.J. and Peters, F.K., 1957, Arch.f.d. Eisenhuttenw, **28**, 567-574

FACT, thermo-chemical database, http://www.crct.polymtl.ca/fact/fact.htm

Folkhard, E., 1988, *Welding metallurgy of stainless steels.* Springer-Verlag Wien, New York, 10

Fresnedo, C. and Ruiz, J.M., 1996, *Change to mechanical descaling.* Wire Journal International, 70 - 73

Fujii, C.T. and Meussner, R.A., 1963, *Oxide structures produced on iron-chromium alloys by a dissociative mechanism.* Journal of the electrochemical society, **110**, 1195 - 1204

Fujii, C.T. and Meussner, R.A., 1964, *The mechanism of high temperature oxidation of iron-chromium alloys in water vapor*, Journal of the electrochemical society, **111**, 1215 - 1221

Fukugawa, T., Okada, H., Maehara, Y., 1994, *Mechanism of red-scale defect formation in Si-added hot-rolled steel sheets.* ISIJ International, **34,** 906 - 911

Fukutsuka, T., Nakamura, T., Sato, M., Kokubo, I. and Ishida, R., 1981, *Study of descaling of steel slabs before hot rolling*, Transactions of the Iron and Steel Institute of Japan, **21**, 699 - 707

Garceau R., 1997, *Mechanical descaling*, Wire Technology International, 63 - 65

Gibbs, G.B., 1981, *On the influence of metal lattice diffusion on oxidation of metals and alloys*, Oxidation of metals, **16**, 147 - 158

Grigg, C.R., Sexton, B.G. and Matteson, L.E., 1985, *1420 mm Hot strip mill control of rolled-in-scale*, 4th International Steel Rolling Conference, **1**, Deauville, France, A39.1 - A39.8

Hindham, H. and Whittle, D.P., 1982, *Microstructure, adhesion and growth kinetics of protective scale on metals and alloys,* Oxidation of metals, **18**, 245 - 284

Hosford, W.F. and Caddell, R.M., 1983, *Metal forming, mechanics and metallurgy*, Prentice-Hall, Englewood Cliffs, NJ.

Ito, M.; Tachibana, R.; Seino, Y.; Yamamoto, A.; Kawabata, Y. and Uchino, K., 1997, *Descaling behaviour of type-430 hot-rolled stainless steel coil*, Japanese Journal of Applied Physics, **36**, 7404 - 7410

Metals Handbook, 1980, American Society for Metals, **3**, 194

Knowlton, J, Caplan, P.E., 1985, *Rotameter Corrections for gas density.* American Industrial Hygiene Association Journal, **46**, B-10 - 16

Kofstad, P., 1988, *High temperature corrosion*, Elsevier, London

Laheij, M.A.J.T.H., van Loo, F.J.J and Metselaar, R., 1980, *Phase relations in the Fe-Cr-O system at 1200°C investigated by means of a diffusion couple technique.* Oxidation of Metals, **14**, 207 - 215

Levin, E.M., Robbins, C.R. and McMurdie, H.F., 1964, *Phase diagrams for ceramists*, The American ceramic society, Columbus, Ohio

Liekmeier F., 1982, *Mechanical descaling of wire rod by bending — Possibilities and limits*, Wire, **32**, 57 - 58

Matsuno, F., 1980, *Blistering and hydraulic removal of scale films of rimmed steel at high temperature*, Transactions of the Iron and Steel Institute of Japan, **20**,

Morris, P., Bagshaw, P. and Marston, H., 1996, *Descaling of steels in rolling mills*, Report EUR 15836, ECSC agreement no. 7210.EA/818, European commission, Technical steel research, Office for official Publications of the European Communities, Luxembourg.

Palin, G.M., August 1965, *Effect of heating conditions on the adhesion of the scale to the metal*, Stal in English, **8**, 677 - 679

Pickens, J.W., 1983, *The microstructure characteristics of oxide scale formed during bar processing*, 21st Mechanical working & steel processing conference, Philadelphia, USA, 26 - 28 Oct. 1983. Iron and Steel Society / AIME, Warrendale, USA, 39 - 65

Pieraggi, B., Rapp, R.A. and Hirth, J.P., 1995, *Role of interfacial defects in oxide scale growth.* Oxidation of Metals, **44**, 63 - 79

Rapp, R.A., 1984, *The high temperature oxidation of metals forming cation-diffusing scales,* Metallurgical Transactions Series B, **15B**, 195-212

Rapp, R.A., 1993, *Fundamental aspects of high-temperature corrosion,* Journal de Physique, Colloque C9, **3**, 1- 15

Sachs, K. and Tuck, C.W., 1968, *Surface oxidation of steel in industrial furnaces*, Proceedings of the conference held in London, 19 -20 December 1967, The iron and steel institute, London, 1 - 17

Sachs, K. and Tuck, C.W., 1970, *Scale growth during re-heating cycles*, Werkstoffe und korrosion, **21**, 945 - 954

Schutze, M., 1995, *Mechanical properties of oxide scales.* Oxidation of Metals, **44**, 29 - 61

Sheasby, J.S., Boggs, W.E. and Turkdogan, E.T., 1984, *Scale growth on steels at 1200 C: rationale of rate and morphology*, Metal science, **18**, 127 - 136

Sheppard, T. and Steen, W.M., 1970, *Hydraulic Descaling of steel: a preliminary experimental survey*, Journal of the Iron and Steel Institute, **7**, 797 - 805

Sheridan, A.T. and Simon, P., 1 February 1995, *Descaling of steels in rolling mills*, European steel-making developments and perspectives in rolling and reheating, Luxembourg, 233 - 244

Taniguchi, S., 1985, *Stress developed during oxidation of metals and alloys*, Transactions of the Iron and Steel Institute of Japan, **25**, 3 - 13

Tominaga, J., Wakimoto, K., Mori, T., Murakami, M., Yoshimura, T., 1982, *Manufacture of wire rods with good descaling property.* Transactions of the Iron and Steel Institute of Japan, **25**, 3 -13

Tuck, C.W. and Barlow, J., 1972, *The effect of reheating furnace atmosphere on the adhesion of scale to steel*, Iron and steel, **45**, 31 - 38

von Bogdandy, L. and Engell, H.J., 1967, *The reduction of iron ores,*Berlin-Heidelberg-New York, 83-89

Whittle, D.P. and Wood, G.C., 1967, *Complex scale formation on an iron-18% chromium alloy.* Journal of the Electrochemical Society, **114**, 986 - 993

Wagner, C., 1959, *Reaktionstypen bei der Oxydation von Legierungen.*, Zeitschrift fur Elektrochemie, **63**, 772-782.

Zittermann, J.A., Bacco, R.P. and Boggs, W.E., April 1982, *Factors affecting scale adhesion on steel forging*, Journal of metals, **34**, 4, 22 - 26

APPENDIX 1

ANALYSIS OF REACTION RATES AND KINETICS OF IRON

A.1.1 Introduction

This appendix presents an analysis of the rate of scale growth. The mechanisms generally observed for the oxidation of iron can be divided into two stages — an initial linear rate of oxidation, followed by a parabolic rate of oxidation. The initial mechanism is observed for short times up to a certain oxide thickness. Initial oxidation rates depend on the oxidizing species and the rate is expressed in terms of the rate of adsorption of the oxidizing species on the scale surface. When the oxide layer reaches a certain thickness, approximately 0.4 mm (Pettit and Wagner, 1964), the mechanism of oxidation becomes controlled by the diffusion of the ionic species through the oxide layer, leading to parabolic oxidation.

A.1.2 Analysis

A.1.2.1 Symbols used

t (s)	Time
x (m)	Scale thickness
$D_{Fe}(m^2/s)$	Self-diffusion coefficient of Fe^{2+} in iron oxides
$A(m^2)$	Surface area of the sample
G (mole/ m^3)	Molar volume of the oxide
K_p (g^2/m^4s)	Parabolic rate constant

ρ_{FeO} (g/m^3)	Density of FeO
M_o (g/ g-mole)	Molecular weight of atomic oxygen
M_{FeO} (g/g-mole)	Molecular weight of FeO
Y	Iron-ion vacancy fractions
β (m/s)	Mass-transfer coefficient
D_{O2} (m^2/s)	Diffusion coefficient of oxygen
u (m/s)	Gas velocity past the sample surface
l (m)	Length of the sample and
ν (m^2/s)	Kinematic gas viscosity.
T(K)	Temperature
R (J/mole K)	Gas constant
P (atm)	Pressure

A.1.2.2 Diffusion in the oxide

The parabolic oxidation mechanism is driven by the diffusion of metal ions and vacancies through the oxide layer and chemical equilibrium is maintained at the metal-oxide and oxide gas boundaries during the course of oxidation (Abuluwefa *et al,* 1996).

The diffusion of Fe^{2+} cations is expressed in terms of Fick's first law,

$$\frac{dn_{Fe}}{Adt} = \frac{3D_{Fe^{2+}}\,\Delta[Fe^{2+}]}{x}$$

Where $x = G\,\Delta n_{Fe}/A$ G = Molar volume of the oxide (m^3/mole Fe)

$$\text{Thus} \quad \frac{dn_{Fe}}{Adt} = \frac{3D_{Fe^{2+}}\Delta[fe^{2+}]}{G\Delta n_{Fe}\,/\,A}$$

$\Delta[Fe^{2+}]$= Concentration of cations in the scale and Δn_{Fe} = moles Fe^{2+}

The exponent 3 in this equation results from the parallel movement of electrons and cations in the scale layer (von Bogdandy and Engell, 1967)

By integration:

$$G\int_0^{\Delta n_{Fe}} dn_{Fe}\Delta n_{Fe} = 3\int_0^t D^* A^2 \Delta[Fe^{2+}]dt$$

$$\frac{\Delta n_{Fe}^2}{A^2} = \frac{6D_{Fe^{2+}}\Delta[Fe^{2+}]t}{G}$$

The parabolic rate constant gives the increase in mass (due to reacted oxygen) as follows:

$(\Delta m/A)^2 = K_p t$

It follows that the parabolic rate constant is given by

$K_p = 6xD_{Fe2+}\Delta[Fe^{2+}]\ M_o^2\ /G$

The molar volume of FeO (G) can be written as $G = M_{FeO}/\rho_{FeO}$

and the concentration of Fe^{2+} ions, $[Fe^{2+}] = \rho_{FeO}(1-y)/\ M_{FeO}$

$$K_p = \frac{6 * D_{Fe^{2+}} * \rho_{FeO}^2 * M_0^2 (y_{FeO/Fe_3O_4} - y_{Fe/FeO})}{M_{FeO}^2} \qquad (A)$$

$y_{FeO/Fe3O4}$ and $y_{Fe/FeO}$ are the iron vacancy fractions at the FeO/Fe_3O_4 and Fe/FeO boundaries respectively. The vacancy concentrations are determined from the wustite-magnetite (y = 0.14) and iron-wustite (y = 0.049) equilibria respectively (Ajersch, 1992). The self-diffusion coefficient (cm^2/s) of Fe^{2+} in FeO can be calculated as below

$D_{Fe2+} = 4.5x10^{-2}exp(-6641/RT)$ (Deich and Oeters, 1973)

By differentiation of $(\Delta m/A)^2 = K_p t$ the following is obtained:

$$2 * \frac{\Delta m}{A} * \frac{d(\Delta m)}{Adt} = K_p$$

Where

$$\frac{\Delta m}{A} = \frac{x\rho_{FeO}M_o}{M_{FeO}} \qquad (x = \text{thickness of scale})$$

Thus

$$\frac{d(\Delta m / A)}{dt} = \frac{K_p M_{FeO}}{2x\rho_{FeO}M_o}$$

This rate of scale growth is matched by molecular oxygen transfer to the scale-gas interface:

$$\frac{d(n_{O2} / A)}{dt} = \frac{K_p M_{FeO}}{x\rho_{FeO}M_{O2}^2} \qquad (B)$$

Where $d(n_{O2}/A)dt$ gives the rate of oxygen transfer to the scale surface. This can be determined as follows:

$$\frac{n_{O2}}{A} = \beta\Delta C_{O2}$$

Thus the oxidation rate in terms of the oxygen mass transfer is:

$$\frac{n_{Fe^{2+}\rightarrow FeO}}{A} = 2 * \beta\Delta C_{O2} = 2 * \beta\Delta P_{O2} / RT \qquad (C)$$

In which β is the mass transfer coefficient (m/s). The equation expressing β for gas-phase mass-transport control is

$$\beta = \frac{4}{3}\frac{D_{O2}}{l}(Re)^{\frac{1}{2}}(Sc)^{\frac{1}{3}}$$

Where Re is the Reynolds number ($u l / \nu$), Sc is the Schmidt number (ν / D_{O2}), u is the gas velocity past the sample surface, l is the length of the sample and ν is the kinematic gas viscosity (Abuluwefa *et al*, 1996).

A.2.3 Application of Analysis

A.2.3.1 Conditions used in analysis

Gas constant, R = 8.314 J/mole K

Furnace temperature, T = 1500 K

Diffusion coefficient of Fe^{2+}, $D_{Fe2+} = 3.98x10^{-10}$ m^2/s

Molecular weight of FeO, $M_{FeO} = 0.07185$ kg/mole

Density of FeO, $\rho_{FeO} = 5883$ kg/m^3

Molecular weight of atomic oxygen, $M_O = 0.016$ kg/mole

Pressure, P = 0.865 atm

Diffusion coefficient of O_2, $D_{O2} = 3.27x10^{-4}$ m^2/s

Length of sample, l = 0.1 m

Gas velocity, u = 0.1 m/s

Kinematic viscosity of the gas, $\nu = 2.3*10^{-4}$ m^2/s

Equilibrium iron vacancy fraction at the Fe/ FeO boundary, $y_{Fe/FeO} = 0.049$

Equilibrium iron vacancy fraction at the FeO/ Fe_3O_4 boundary, $y_{FeO/Fe3O4} = 0.14$

Using the above data, the parabolic rate constant (K_p) was calculated as $3.7*10^{-4}$ kg^2/m^4s which is in the same range as the value ($3.11*10^{-4}$ kg^2/m^4s) calculated by Sachs and Tuck (1970). Using equation B, the rate of mass transfer of Fe^{2+} was calculated for various scale thicknesses and the graph below shows the relation between the oxidation rate and the scale thickness.

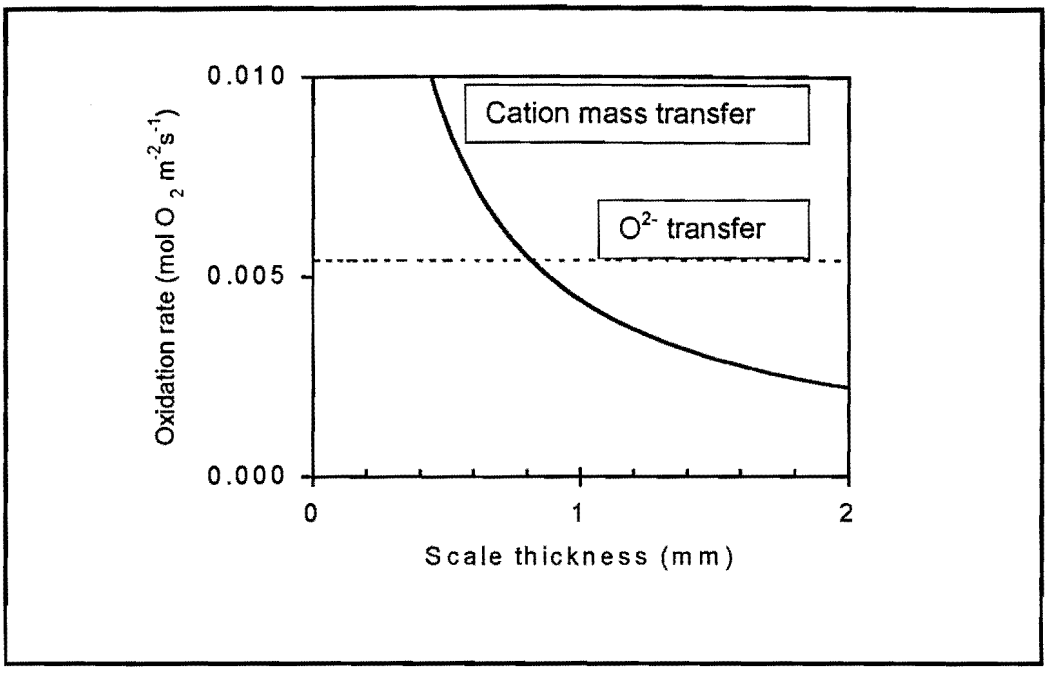

The dotted line represents the situation where oxygen mass transfer is the limiting case and the solid graph represents where cation mass transfer is the limiting case. From the above graph, it can be seen that FeO is present up to a thickness of between 0.4 and 0.5 mm, beyond this thickness, the rate-controlling step becomes the arrival of Fe^{2+} at the interface.

The overall oxidation rate is illustrated in the figure below:

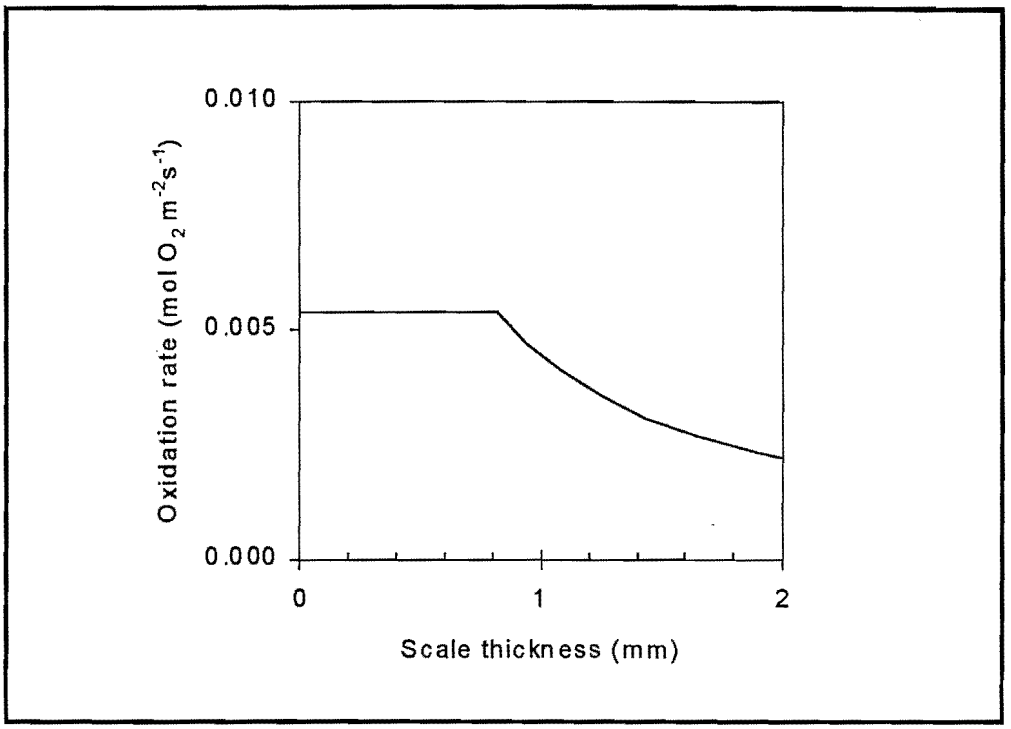
0.010
0.005
0.000
Oxidation rate (mol O_2 $m^{-2}s^{-1}$)
0
1
2
Scale thickness (mm)

APPENDIX 2

THEORETICAL ANALYSIS OF POSSIBLE MECHANISMS OF HYDRAULIC DESCALING

A.2.1 Introduction

This appendix presents an analysis of descaling mechanisms. Each of these mechanisms has been considered as being independent, thus avoiding the complication that would otherwise follow from possible interactions between them. It is recognized that synergistic interactions may arise in practice. This analysis is largely taken from Morris *et al*, (1996).

A.2.2 Analysis

A.2.2.1 Symbols used

P (Pa)	Impact pressure of descaling jet
T	Temperature
ρ (kg/m^3)	Density of water
G (m^3/s)	Volume flow rate of water
t (m)	Thickness of jet
B (m)	Width of steel being descaled
v (m/s)	Speed of steel under jet
θ (^{0})	Angle of jet from vertical
ρ_s (kg/m^3)	Density of scale

α ($°C^{-1}$)	Coefficient of thermal expansion of scale
°C (J/kg °C)	Specific heat capacity of scale
E (N/m^2)	Elastic modulus of scale
K (W/m °C)	Thermal conductivity of scale
x (m)	Thickness of scale
l (m)	Distance between through scale cracks
σ (J/m^2)	Energy required to separate scale from steel
ε_c	Compressive strain to failure of scale
ε_T	Tensile strain to failure of scale
J (N/m^2)	Shear strength of scale / metal interface

A.2.2.2 Effect of thermal shock on scale

Some quantitative indication of whether thermal shock is a feasible mechanism can be obtained by estimating the time required to cool the scale to a depth. Assuming that conduction through the scale is rate determining, the time to cool the scale is of the order of l^2/α, where *l* is the scale thickness and α, the thermal diffusivity.

The time that the steel takes to traverse the thickness of the jet = t/v. This is the minimum time for which the scale would experience a cooling effect from the water; the real time will be longer than this owing to spreading of the water over the scale. The thickness of scale, which would be cooled, can therefore be estimated as:

$$\left(\frac{K}{p_s C}\frac{t}{v}\right)^{\frac{1}{2}} \qquad \text{(A3.1)}$$

If this distance is less than the total scale thickness (quantitatively tested in section A.1.3.2), then the scale / metal interface will not be directly cooled by the jet. There

will be contraction stresses in the outer layers of the scale, which would lead to fracture of the scale, with de-cohesion taking place by a shear effect leading to tensile forces across the scale / metal interface.

A.2.2.3 Effect of deformation of scale

The vertical component of the pressure of the water jet on the scale may crush and shatter the scale, following which the pieces of scale are removed by the water.

Compressive stress on scale = vertical component of pressure jet = P Cos θ

Compressive strain in steel = (P/E) Cos θ

The condition for descaling by this mechanism is:

$$(P/E)\ \text{Cos}\ \theta > \varepsilon_c \quad \ldots\ldots\ldots\ldots\ldots\ldots\ldots\ldots\ldots\ldots\ldots\text{A3.2}$$

This assumes that the pressure exerted by the jet is uniform over its entire area of impact.

A.2.3 Application of Analysis

A.2.3.1 Conditions used in analysis

Density of water, ρ = 1000Kg/m^3

Molecular weight of water, m = 18 g/mole

Density of FeO at 1000°C, ρ_s = 5500 kg/m^3

Heat capacity of scale, C_p = 65J/K (FACT, 1988)

Thermal diffusivity, = 8.3 * 10^{-7} m^2/s (in the vicinity of 1100°C)

Thermal conductivity of scale, k = 4.2 W/ m K (Akiyama *et al*, 1992)

Quantities relating to mechanical properties of scale at rolling temperatures are not very well known. Estimates of their likely magnitudes can however be obtained from published work.

Coefficient of expansion, $\alpha = 13.5 * 10^{-6} {}^{o}C^{-1}$ (this is the average values for FeO and Fe_2O_3)

Elastic modulus of scale, $E = 18*10^4$ MN m^{-2} (from Hancock *et al.,* 1974)

Tensile strain to failure, $\varepsilon_T = 2.3*10^{-4}$ (Hancock P., 1980)

Compressive strain to failure, $\varepsilon_c = 40*10^{-4}$ (no reference available. An estimate of the probable magnitude of ε_c, has therefore been made based on (Hancock, 1980)

Energy required to fracture scale / metal interface = 1 J/m (estimate, no reference found)

Shear strength of scale/metal interface, J = 20 MN m^{-2} (estimate based on the fact that tensile strengths of the interface of this order have been measured at room temperatures, (Hancock *et al.,* 1974).

For typical commercial practice,

Impact pressure, $P = 1*10^6$ Pa

Volume flow rate, $G = 1*10^{-3}$ m^3/s

Thickness of jet, $t = 8*10^{-3}$ m

Width of steel, B = 0.1 m (assuming descaling of a billet)

Speed of steel, v = 1 ms^{-1}

Angle of jets from vertical, $\theta = 15^0$ (a typical value, although higher angles are used in some mills).

A.2.3.2 Effects of thermal shock on scale

Using literature values for the thermal conductivity and density of wustite (Akiyama *et al*, 1992) and its heat capacity (FACT, 1998), the thermal diffusivity is estimated to be some $8.3*10^{-7}$ m^2/s in the vicinity of 1100°C. Based on the typical thickness of the jet of around 8 mm, and slab speeds of 0.1 to 1 m/s (Morris *et al*, 1996), the time that the scale is exposed to the water jet is between 8 and 80 ms — which, based on the thermal diffusivity, is only sufficient time to quench the outer 80 - 250 μm of the scale (compared with the total scale thickness which may be 2 mm or more after reheating). This very limited cooling of the scale does bring the validity of the thermal shock mechanism into doubt.

Equation A3.1 gives the depth of scale, which would experience cooling as a result of the effects of the water jets. This expression is calculated to be 0.2 mm. This assumes that the cooling effect lasts only as long as the steel is under the water jets, which is an unrealistic assumption since water lying on the surface of the scale will continue to cool it. It appears, however, that the scale/ metal interface is unlikely to be cooled if the scale is more than a few millimeters thick, and therefore under these circumstances the scale removal mechanism cannot depend on uniform cooling of the scale. Tensile stresses in the scale surface, caused by cooling of the outer layer of the scale, must however lead to the generation of compressive stresses in the lower layers of the scale, resulting in a shear stress at the scale / metal interface.

A.2.3.3 Effect of deformation of scale

Equation A3.2 gives the condition for descaling to take place by crushing of the scale. It can be seen that this mechanism is expressly dependent on the impact pressure generated by the descaling system. Therefore, calculating the left-hand side we have:

APPENDIX 3

REQUIRED GAS FLOW RATES IN FURNACE

Introduction

The gas composition was chosen to simulate the combustion of CH_4 with air, with 3% or 4% excess free oxygen as shown in the calculations below. In this specific example, the gas composition was calculated using 3% excess oxygen.

	CH_4	$+ 2O_2$	$+ N_2$	=	CO_2	$+ 2H_2O$	$+ N_2$	$+ O_2$
MM	16	32	28		44	18	28	32
Moles	1	2	7.5		1.0	2.0	8.9	0.4

Using "goal seek" the % excess oxygen that must enter to ensure that 3% excess O_2 is obtained in the exit gas, can be calculated.
Thus for a calculated 18.4 % O_2 entering, the rest of the mass balance is as follows:

CH_4	$+ 2O_2$	$+ N_2$	=	CO_2	$+ 2H_2O$	$+ N_2$	$+ O_2$
	2.4	8.9		8.1	16.3	72.6	3.0

The total volume of gas flowing through the furnace is then calculated as follows:

Dimensions of tube (cm)

Outside	Inside	Length (cm)	
9	7.6	100	
Area (πr^2)	0.0045	m^2	r = inside radius of tube
Vtot	8E-05	Nm^3/s	Vtot = total volume of gas (area x velocity)

Where the gas velocity is 0.1m/s.

Thus the flow rates of the individual gases through the furnace should be:

	Nm^3/s	L/min	Mole/s
VN_2	6E-05	3.59	0.0024
VO_2	2E-06	0.15	0.0001
VCO_2	7E-06	0.40	0.0003

The following tables show the rotameter calibration values of the various gases using the soap bubble meter.

Nitrogen calibration

Pressure drop	Rotameter Nr.	ml	time	ml	time	ml	time	ml	time	ml	time	l/min
85	1	100	4.37	100	4.2	100	4.36	200	8.65	200	8.65	1.39
108	2	100	2.34	100	2.34	100	2.34	200	4.85	200	4.82	2.53
122	3	100	1.66	100	1.57	100	1.58	200	3.23	200	3.28	3.72
143	4	100	1.2	100	1.16	100	1.18	200	2.35	200	2.38	5.08
162	5	100	0.87	100	0.84	100	0.85	200	1.85	200	1.82	6.84

Rotameter Nr.	measured rate	Rotameter Nr.	rate using equation
1	1.39	1	1.22
2	2.53	2	2.57
3	3.72	3	3.91
4	5.08	4	5.26
5	6.84	5	6.60

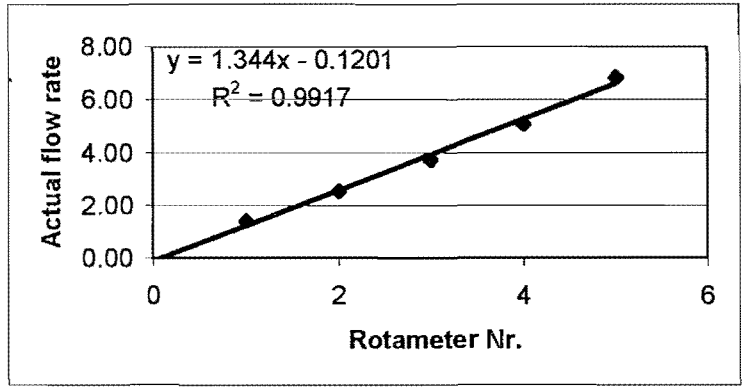

APPENDIX

Oxygen calibration

Pressure drop	Rotameter nr.	ml	time	ml	time	ml	time	ml	time	ml	time	l/min
mmHg												
87	220	15	3.45	20	4.85	15	3.66	20	4.82	15	3.48	0.25
87	200	15	3.81	20	5.08	10	2.48	15	3.81	20	5.11	0.24
86	150	15	5.05	20	6.62	15	5.04	20	6.64	20	6.61	0.18
80	100	15	7.94	15	7.74	10	5.22	15	7.91	10	5.1	0.12
76	50	10	9.48	10	9.4	15	14.19	15	14.18	10	9.2	0.06
		10	9.34	15	14.05	10	9.46	15	14.18	15	14.5	0.06

Rotameter Nr.	measured rate
220	0.25
200	0.24
150	0.18
100	0.12
50	0.06

Rotameter Nr.	rate using equation
220	0.264
200	0.24
150	0.18
100	0.12
50	0.06

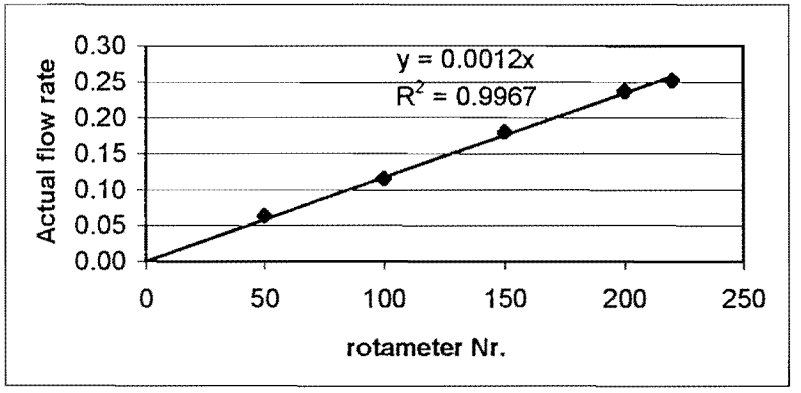

CO_2
calibration

Pressure drop	rotameter nr.	ml	time	ml	time	ml	time	ml	time	ml	time	l/min
(mmHg)	50	100	70.51	100	70.31	100	69.21	100	69.27	100	68.73	0.09
	100	100	42.53	100	42.44	100	42.56	100	42.31	100	42.1	0.14
	150	100	31.6	100	31.54	100	31.61	200	61.23	100	30.5	0.19
84	200	25	5.1	25	5.05	30	6.21	30	6.27	30	6.22	0.29
	250	100	16.59	200	33.36	100	16.81	200	33.17	200	33.26	0.36
88	300	25	3.53	25	3.58	30	4.34	25	4.32	30	3.6	0.42
	350	100	12.53	200	24.73	100	12.13	200	24.41	100	12.33	0.49
91	400	25	2.91	30	3.44	30	3.52	30	3.46	25	2.99	0.51
96	500	25	2.39	25	2.42	30	2.86	25	2.34	30	2.89	0.63
101	600	35	3.02	35	3.11	35	3	30	2.56	20	1.72	0.69

rotamete nr.	measured rate	rotameter nr.	rate using equation
50	0.09	50	0.65
100	0.14	100	1.3
150	0.19	150	1.95
200	0.29	200	2.6
250	0.36	250	3.25
300	0.42	300	3.9
350	0.49	350	4.55
400	0.51	400	5.2
500	0.63	500	6.5
600	0.70	600	7.8

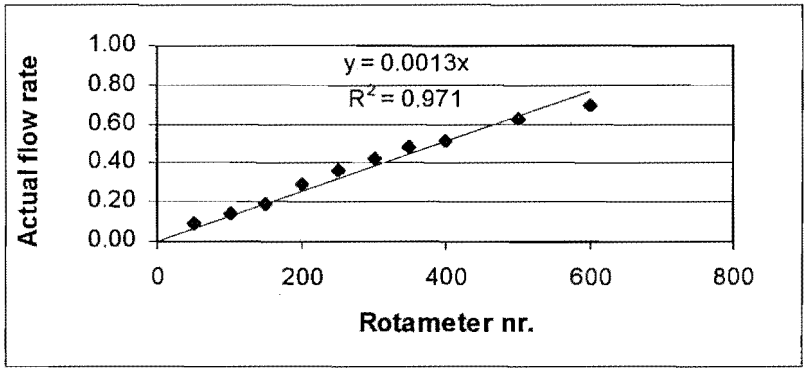

Rotameter corrections for gas density were done since changes in gas density could significantly affect the airflow measurements by rotameters. Using a rotameter at an altitude different than that, for which it was calibrated, could yield serious error. From the observed flow rate at the bubble tower (V1), the flow rate at the rotameter (V2) at 0.865 atm could be calculated using the following equation

Flow rate through rotameter (V2) = (P_{atm} / P_{rot}) x Observed flow rate (V1)

V3 – the flow rate at the rotameter at 1 atm was then calculated and as a check, V2 was then recalculated as shown below.

$$R_2 = R_1\sqrt{\frac{P_2}{P_1}}$$

Where R is the rotameter reading and P is the pressure.

N2

Patm = 87624.5 P3 = 101300 T(K) = 298

rotameter setting	Prot mmHg	Pabs Pa	V1 at bubble tower (l/min)	V2 at rotameter = V1*Patm/prot	V3 at rot at 1atm = V2/sqrt(Prot/P3)	V2 at rot = V3/sqrt(P3/P2)		n (mol/s) ProtV2/RT
1	85	98954	1.39	1.23	1.25	1.23		0.00082
2	108	102020	2.53	2.17	2.17	2.17		0.00149
3	122	103886	3.72	3.14	3.10	3.14		0.00219
4	143	106685	5.08	4.17	4.07	4.17		0.00300
5	162	109217	6.84	5.48	5.28	5.48		0.00403

O2

Patm = 87624.5 P3 = 101300 T(K) = 298

rotameter setting	Prot mmHg	Pabs Pa	V1 at bubble tower (l/min)	V2 at rotameter V1*Patm/prot	V3 at rot at 1atm V2/sqrt(Prot/P3)	V2 at rot V3/sqrt(P3/P2)		n (mol/s) ProtV2/RT
220	87	99221	0.25	0.22	0.23	0.22		0.00015
200	87	99221	0.24	0.21	0.21	0.21		0.00014
150	86	99087	0.18	0.16	0.16	0.16		0.00011
100	80	98288	0.12	0.10	0.10	0.10		0.00007
50	76	97755	0.06	0.06	0.06	0.06		0.00004

CO2

Patm = 87624.5 P3 = 101300 T(K) = 298

rotameter setting	Prot mmHg	Pabs Pa	V1 at bubble tower (l/min)	V2 at rotameter V1*Patm/prot	V3 at rot at 1atm V2/sqrt(Prot/P3)	V2 at rot V3/sqrt(P3/P2)		n (mol/s) ProtV2/RT
200	84	98821	0.19	0.17	0.17	0.17		0.000113
300	88	99354	0.36	0.32	0.32	0.32		0.000212
400	91	99754	0.49	0.43	0.43	0.43		0.000287
500	96	100420	0.51	0.45	0.45	0.45		0.000303
600	101	101087	0.63	0.54	0.55	0.54		0.000370

Patm atmospheric pressure
Pabs absolute pressure
Prot measured pressure at rotameter

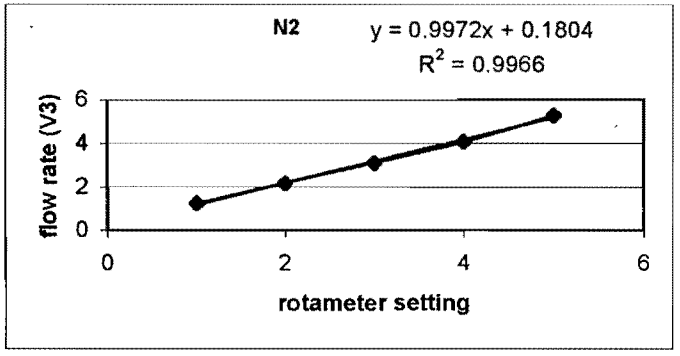

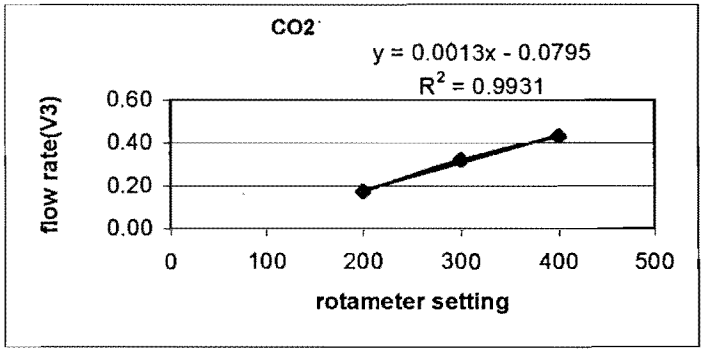

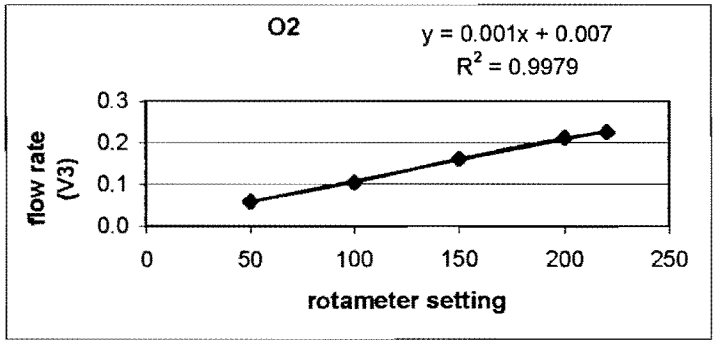

APPENDIX

Thus from the above calculations and graphs, it follows that for a given rotameter setting, the flow rate at the rotameter at 1 atm, can be calculated.

N2

Patm =	101300	pa				T(K) =	298
rotameter setting	Prot mmHg		Pabs Pa	V3 at 1atm	V2 at Pabs V3*sqrt(Prot/Patm)		n at Pabs
3.42	141		120093.8	3.59	3.91		0.00316

O2

Patm =	101300	pa				
rotameter setting	Prot mmHg		Pabs Pa	V3 at 1atm	V2 at Pabs V3*sqrt(Prot/Patm)	n at Pabs
142	141		120093.8	0.15	0.16	0.000131

CO2

Patm =	101300	pa				
rotameter setting	Prot mmHg		Pabs Pa	V3 at 1atm	V2 at Pabs V3*sqrt(Prot/Patm)	n at Pabs
372	141		120093.8	0.40	0.44	0.000355

Patm	atmospheric pressure
Pabs	absolute pressure
Prot	pressure at rotameter

APPENDIX 4

EXPERIMENTAL GAS ANALYSES AND WATER CONTENT

The calculated inlet gas compositions for:

3% excess O_2 in the exit gas is: 3.6 % O_2, 86.7% N_2, and 9.7% CO_2

4% excess O_2 in the exit gas is: 4.7 % O_2, 86.2% N_2, and 9.1% CO_2

16-05-2000

Calibration of inlet gas for 3% excess O_2 in exit gas

	%	%	%	%	%	%
O_2	3.51	3.41	3.27	3.23	3.17	3.12
N_2	88.31	87.92	88.8	88.22	88.33	88.41
CO_2	8.19	8.66	8.55	8.55	8.5	8.47

Calibration of inlet gas for 4% excess O_2 in exit gas

	%	%	%	%	%	%
O_2	4.28	4.31	4.42	4.34	4.29	4.37
N_2	88.07	87.95	87.88	87.89	87.98	87.75
CO_2	7.65	7.74	7.69	7.76	7.73	7.87

23-05-2000

Calibration of inlet gas for 3% excess O_2 in exit gas

	%	%	%	%	%	%	%	%	%
O_2	3.09	3.13	2.97	2.9	2.88	2.88	3.15	2.96	2.96
N_2	88.58	88.61	88.67	88.81	88.86	88.88	88.62	88.82	88.77
CO_2	8.34	8.26	8.36	8.28	8.26	8.24	8.23	8.22	8.27

Calibration of inlet gas for 4% excess O_2 in exit gas

	%	%	%	%	%	%
O_2	4.26	4.28	4.27	4.28	4.29	4.26
N_2	87.78	87.72	87.74	88.08	87.96	87.76
CO_2	7.96	8.01	7.98	7.65	7.75	7.98

15-09-2000

Calibration of inlet gas for 3% excess O_2 in exit gas

	%	%	%	%	%	%	%
O_2	3.48	3.53	3.47	3.54	3.49	3.53	3.61
N_2	86.96	86.4	86.75	86.93	86.74	68.84	86.64
CO_2	9.56	10.07	9.78	9.54	9.77	9.64	9.74

Calibration of inlet gas for 4% excess O_2 in exit gas

	%	%	%	%	%
O_2	4.94	4.88	4.91	4.86	4.79
N_2	86.1	85.88	85.93	86.08	86.29
CO_2	8.95	9.24	9.15	9.06	8.92

Water content of gas mixture

Some preliminary experiments were done to ensure that the correct amount of vapour entered the furnace. This was done by passing the exit gas at the bottom of the furnace through a drierite column that had been pre-weighed. After the experiment the drierite column was then weighed again. The difference between the two weights, gave the amount of water that had been absorbed by the drierite.

mass drierite (g)	376.08
drierite +water	397.57
water (g)	21.49

This value (21.49g, in this case) was then compared to the theoretically calculated mass of water that was expected to be in the gas mixture at the laboratory temperature and pressure.

Total gas flow rate (l/min)	Time (min)	Total gas volume (l)	Temperature (K)	Pressure (Pa)	Moles of gas
5	30	150	299	87624.5	5.287

The moles of gas (N_2, O_2 and CO_2) above, was calculated from the ideal gas law.

% Water in final gas mixture	Moles of water	Mass (g) of water	
16.3	1.030	18.53	

The % water in the gas mixture was calculated as shown in appendix 3. The moles of water was then calculated as follows:

[5.287 / (1- 16.3 / 100)] * (16.3 / 100) = 1.03 moles

In all of the experiments the mass of water (theoretical and measured) were quite similar, as in the above example.

APPENDIX 5

PHASE ANALYSIS COMPOSITIONS OF METAL AND SCALE

The phase analyses of some of the samples are given below:

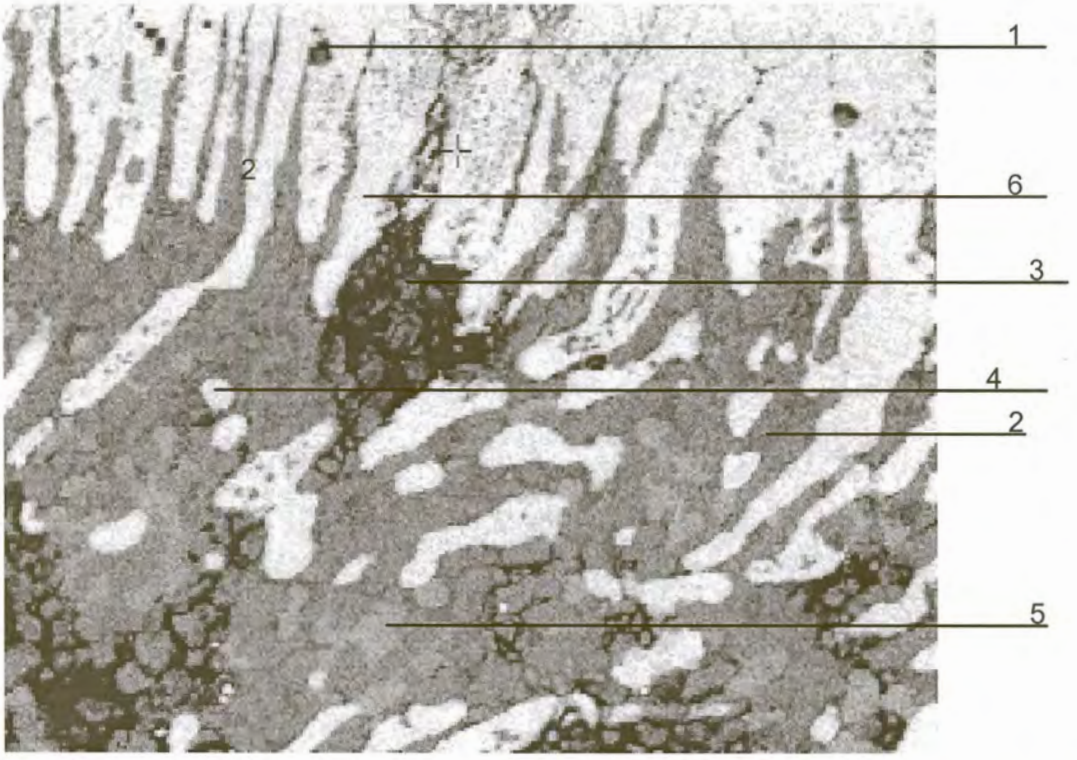

The above diagram shows the structure of scale for type 412 stainless steel reheated at 1210^0C in an atmosphere with 4% excess oxygen for 6hr. The analyses of the different phases are given below.

Point 1

Tue Oct 31 06:58:06 2000

Filter Fit Method
Chi-sqd = 2.11 Livetime = 73.0 Sec.

Element	k-ratio (calc.)	ZAF	Atom %	Element Wt %	Wt % Err. (3-Sigma)
Fe-K	0.2683	1.067	26.55	28.62	+/- 1.98
Ni-K	0.0000	1.051	0.00	0.00	+/- 0.00
Cr-K	0.5067	1.000	50.48	50.67	+/- 2.38
Mn-K	0.0062	1.041	0.61	0.65	+/- 1.30
Si-K	0.0065	1.332	1.59	0.86	+/- 0.24
Ti-K	0.2080	0.923	20.77	19.20	+/- 1.27
Total			100.00	100.00	

Point 2

Filter Fit Method
Chi-sqd = 2.60 Livetime = 84.0 Sec.

Element	k-ratio (calc.)	ZAF	Atom %	Element Wt %	Wt % Err. (3-Sigma)
Fe-K	0.1620	1.075	15.78	17.41	+/- 1.54
Ni-K	0.0050	1.049	0.45	0.52	+/- 1.04
Cr-K	0.4083	1.037	41.25	42.35	+/- 2.14
Mn-K	0.0081	1.061	0.79	0.86	+/- 1.15
Si-K	0.0066	1.292	1.53	0.85	+/- 0.21
Ti-K	0.4005	0.949	40.19	38.01	+/- 1.52
Total			100.00	100.00	

Point 3

Chi-sqd = 2.25 Livetime = 73.0 Sec.

Element	k-ratio (calc.)	ZAF	Atom %	Element Wt %	Wt % Err. (3-Sigma)
Fe-K	0.4817	1.045	48.55	50.34	+/- 2.45
Ni-K	0.0000	1.052	0.00	0.00	+/- 0.00
Cr-K	0.5048	0.940	49.13	47.44	+/- 2.24
Mn-K	0.0196	1.019	1.96	2.00	+/- 1.28
Si-K	0.0010	1.393	0.28	0.15	+/- 0.23
Ti-K	0.0008	0.892	0.08	0.07	+/- 0.36
Total			100.00	100.00	

Point 4

Filter Fit Method
Chi-sqd = 2.39 Livetime = 47.0 Sec.

Element	k-ratio (calc.)	ZAF	Atom %	Element Wt %	Wt % Err. (3-Sigma)
Fe-K	0.9667	1.001	96.67	96.77	+/- 4.03
Ni-K	0.0109	1.055	1.10	1.15	+/- 1.18
Cr-K	0.0256	0.797	2.19	2.04	+/- 0.89
Mn-K	0.0004	1.019	0.04	0.04	+/- 0.73
Si-K	0.0000	1.468	0.01	0.00	+/- 0.20
Ti-K	0.0000	0.918	0.00	0.00	+/- 0.00
Total			100.00	100.00	

Point 5

Chi-sqd = 0.98 Livetime = 77.0 Sec.

Element	k-ratio (calc.)	ZAF	Atom %	Element Wt %	Wt % Err. (3-Sigma)
Fe-K	0.4509	1.050	45.48	47.32	+/- 3.25
Ni-K	0.0000	1.052	0.00	0.00	+/- 0.00
Cr-K	0.5448	0.946	53.19	51.53	+/- 2.29
Mn-K	0.0081	1.019	0.81	0.83	+/- 1.30
Si-K	0.0014	1.388	0.37	0.20	+/- 0.22
Ti-K	0.0014	0.888	0.14	0.12	+/- 0.35
Total			100.00	100.00	

Point 6

Filter Fit Method
Chi-sqd = 2.46 Livetime = 36.0 Sec.

Element	k-ratio (calc.)	ZAF	Atom %	Element Wt %	Wt % Err. (3-Sigma)
Fe-K	0.9665	1.001	96.56	96.78	+/- 4.69
Ni-K	0.0093	1.055	0.93	0.98	+/- 1.22
Cr-K	0.0266	0.797	2.27	2.12	+/- 0.57
Mn-K	0.0000	1.019	0.00	0.00	+/- 0.00
Si-K	0.0008	1.468	0.23	0.12	+/- 0.23
Ti-K	0.0000	0.918	0.00	0.00	+/- 0.00
Total			100.00	100.00	

The next diagram below shows the structure of scale for type 304 stainless steel reheated at 1280^0C in an atmosphere with 3% excess oxygen for 6hr. The analyses of the different phases are also given below. Points 1 and 2 show the compositions of the metal at the scale-metal interface, whilst points 3, 4 and 7 actually show the composition of the chromium-depleted metal within the scale.

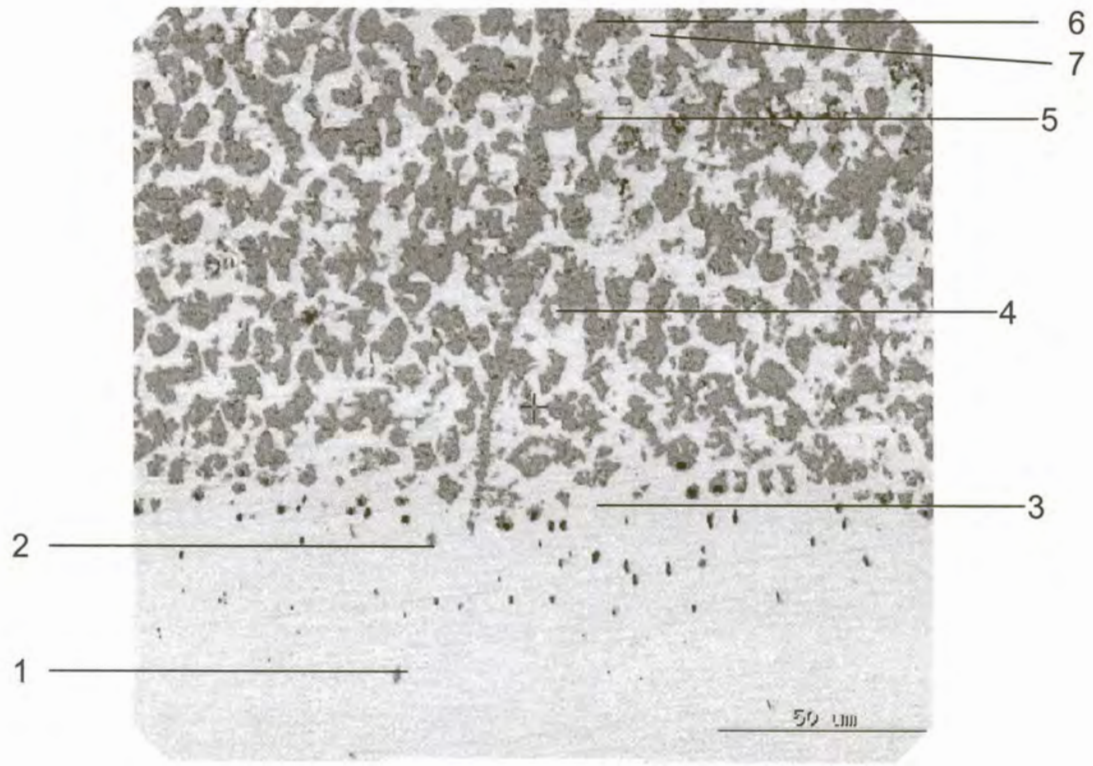

Point 1

Chi-sqd = 4.84 Livetime = 56.0 Sec.

Element	k-ratio (calc.)	ZAF	Atom %	Element Wt %	Wt % Err. (3-Sigma)
Fe-K	0.1923	1.045	19.12	20.09	+/- 2.04
Mn-K	0.2712	1.023	26.85	27.76	+/- 2.23
Si-K	0.0017	1.418	0.46	0.24	+/- 0.16
Cr-K	0.4074	0.986	41.06	40.17	+/- 1.65
Ni-K	0.0238	1.051	2.26	2.50	+/- 0.93
Ti-K	0.1027	0.900	10.25	9.24	+/- 0.71
Total			100.00	100.00	

Point 2

Chi-sqd = 2.27 Livetime = 48.0 Sec.

Element	k-ratio (calc.)	ZAF	Atom %	Element Wt %	Wt % Err. (3-Sigma)
Fe-K	0.4463	1.037	43.31	46.27	+/- 2.50
Mn-K	0.1185	1.023	11.54	12.12	+/- 2.00
Si-K	0.0309	1.464	8.41	4.52	+/- 0.23
Cr-K	0.3393	0.943	32.17	31.99	+/- 1.51
Ni-K	0.0461	1.060	4.35	4.89	+/- 2.02
Ti-K	0.0022	0.922	0.23	0.21	+/- 0.26
Total			100.00	100.00	

Point 3

Chi-sqd = 2.42 Livetime = 33.0 Sec.

Element	k-ratio (calc.)	ZAF	Atom %	Element Wt %	Wt % Err. (3-Sigma)
Fe-K	0.7481	1.010	74.80	75.54	+/- 2.89
Mn-K	0.0027	1.016	0.27	0.27	+/- 0.75
Si-K	0.0017	1.538	0.53	0.27	+/- 0.17
Cr-K	0.1753	0.875	16.32	15.35	+/- 1.12
Ni-K	0.0811	1.057	8.08	8.57	+/- 1.34
Ti-K	0.0000	0.932	0.00	0.00	+/- 0.00
Total			100.00	100.00	

Point 4

Chi-sqd = 3.76 Livetime = 39.0 Sec.

Element	k-ratio (calc.)	ZAF	Atom %	Element Wt %	Wt % Err. (3-Sigma)
Fe-K	0.8241	0.994	81.80	81.91	+/- 2.65
Mn-K	0.0009	1.014	0.10	0.09	+/- 0.56
Si-K	0.0030	1.568	0.94	0.47	+/- 0.27
Cr-K	0.0505	0.840	4.55	4.25	+/- 0.72
Ni-K	0.1258	1.055	12.61	13.28	+/- 1.41
Ti-K	0.0000	0.938	0.00	0.00	+/- 0.00
Total			100.00	100.00	

Point 5

Chi-sqd = 1.73 Livetime = 41.0 Sec.

Element	k-ratio (calc.)	ZAF	Atom %	Element Wt %	Wt % Err. (3-Sigma)
Fe-K	0.4060	1.058	40.69	42.96	+/- 1.95
Mn-K	0.0187	1.022	1.84	1.91	+/- 1.14
Si-K	0.0119	1.445	3.24	1.72	+/- 0.38
Cr-K	0.5496	0.955	53.40	52.50	+/- 1.98
Ni-K	0.0079	1.060	0.75	0.84	+/- 1.08
Ti-K	0.0008	0.896	0.08	0.07	+/- 0.30
Total			100.00	100.00	

Point 6

Chi-sqd = 1.81 Livetime = 31.0 Sec.

Element	k-ratio (calc.)	ZAF	Atom %	Element Wt %	Wt % Err. (3-Sigma)
Fe-K	0.4025	1.059	40.68	42.60	+/- 2.23
Mn-K	0.0174	1.020	1.72	1.78	+/- 1.32
Si-K	0.0049	1.446	1.33	0.70	+/- 0.23
Cr-K	0.5699	0.954	55.77	54.38	+/- 2.33
Ni-K	0.0045	1.059	0.43	0.47	+/- 1.16
Ti-K	0.0007	0.891	0.07	0.06	+/- 0.34
Total			100.00	100.00	

Point 7

Chi-sqd = 3.34 Livetime = 32.0 Sec.

Element	k-ratio (calc.)	ZAF	Atom %	Element Wt %	Wt % Err. (3-Sigma)
Fe-K	0.8138	0.988	80.83	80.42	+/- 2.98
Mn-K	0.0001	1.012	0.01	0.01	+/- 0.60
Si-K	0.0007	1.581	0.23	0.11	+/- 0.17
Cr-K	0.0317	0.838	2.87	2.66	+/- 0.43
Ni-K	0.1596	1.053	16.06	16.80	+/- 1.72
Ti-K	0.0000	0.940	0.00	0.00	+/- 0.00
Total			100.00	100.00	

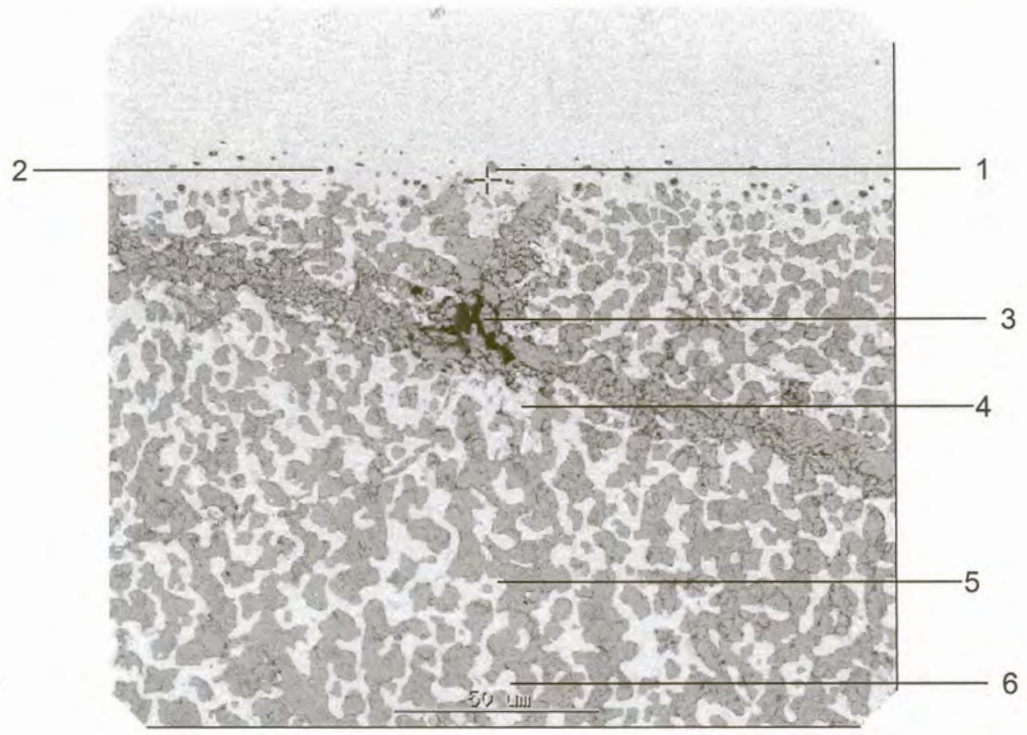

The above diagram shows the structure of scale for type 304 stainless steel reheated at 1260^0C in an atmosphere with 3% excess oxygen for 6hr. The analyses of the different phases are given below.

mon 30/10 Point 1

Element	k-ratio (calc.)	ZAF	Atom %	Element Wt %	Wt % Err. (3-Sigma)
Si-K	0.0057	1.350	1.46	0.77	+/- 0.33
Fe-K	0.0508	1.041	5.03	5.29	+/- 1.83
Cr-K	0.4982	0.987	50.25	49.19	+/- 3.31
Ni-K	0.0000	1.043	0.00	0.00	+/- 0.00
Mn-K	0.4423	1.012	43.26	44.75	+/- 4.44
Total			100.00	100.00	

Mon Oct 30 10:34:50 2000
Point 2
Filter Fit Method
Chi-sqd = 1.60 Livetime = 80.0 Sec.

Element	k-ratio (calc.)	ZAF	Atom %	Element Wt %	Wt % Err. (3-Sigma)
Si-K	0.0177	1.415	4.76	2.51	+/- 0.37
Fe-K	0.4771	1.031	46.90	49.18	+/- 2.82
Cr-K	0.3555	0.934	34.01	33.20	+/- 1.70
Ni-K	0.0467	1.052	4.46	4.91	+/- 2.24
Mn-K	0.1001	1.019	9.89	10.20	+/- 2.19
Total			100.00	100.00	

Point 3

Filter Fit Method
Chi-sqd = 3.51 Livetime = 70.0 Sec.

Element	k-ratio (calc.)	ZAF	Atom %	Element Wt %	Wt % Err. (3-Sigma)
Si-K	0.0015	1.468	0.42	0.21	+/- 0.23
Fe-K	0.8972	1.007	89.67	90.32	+/- 3.01
Cr-K	0.0944	0.829	8.34	7.83	+/- 1.16
Ni-K	0.0127	1.056	1.27	1.34	+/- 1.19
Mn-K	0.0029	1.019	0.30	0.30	+/- 0.86
Total			100.00	100.00	

Point 4

Filter Fit Method
Chi-sqd = 3.40 Livetime = 60.0 Sec.

Element	k-ratio (calc.)	ZAF	Atom %	Element Wt %	Wt % Err. (3-Sigma)
Si-K	0.0007	1.510	0.22	0.11	+/- 0.17
Fe-K	0.8075	0.987	80.14	79.73	+/- 3.13
Cr-K	0.0342	0.834	3.08	2.85	+/- 0.46
Ni-K	0.1643	1.047	16.44	17.19	+/- 2.87
Mn-K	0.0012	1.011	0.13	0.12	+/- 0.63
Total			100.00	100.00	

Point 5

Filter Fit Method
Chi-sqd = 3.21 Livetime = 59.0 Sec.

Element	k-ratio (calc.)	ZAF	Atom %	Element Wt %	Wt % Err. (3-Sigma)

Si-K	0.0005	1.511	0.15	0.08	+/- 0.18
Fe-K	0.8075	0.987	80.14	79.67	+/- 2.46
Cr-K	0.0314	0.833	2.82	2.61	+/- 0.79
Ni-K	0.1686	1.046	16.88	17.64	+/- 1.85
Mn-K	0.0000	1.010	0.00	0.00	+/- 0.00
Total			100.00	100.00	

Point 6

Chi-sqd = 2.38 Livetime = 56.0 Sec.

Element	k-ratio (calc.)	ZAF	Atom %	Element Wt %	Wt % Err. (3-Sigma)
Si-K	0.0758	1.412	19.09	10.69	+/- 0.69
Fe-K	0.7158	1.029	66.13	73.68	+/- 4.11
Cr-K	0.1233	0.888	10.55	10.95	+/- 1.48
Ni-K	0.0078	1.069	0.72	0.84	+/- 1.26
Mn-K	0.0370	1.039	3.51	3.84	+/- 1.20
Total			100.00	100.00	

APPENDIX 6

CALCULATION OF AVERAGE RESIDUAL SCALE THICKNESS

A.6.1 Introduction

The average residual scale thicknesses were calculated using tools on the scanning electron microscope.
The frame area, fraction of scale as well as the width of the scale were measured using the SEM and then the scale area was calculated according to the following:

Scale area = frame area x fraction of scale

The average residual scale was then determined as follows:

Residual scale = scale area / scale width

The results for the various samples are given below.

412								
					residual	residual		
conditions	scale fraction	frame area	scale area	scale width (um)	thickness (um)	thickness (mm)	averages (mm)	
6hr, 1280C, 3% O2	0.04629	7785100	360372.279	2790.2	129.16	0.13		
	0.04595	7785100	357725.345	2792.09	128.12	0.13		
	0.03343	7785100	260255.893	2804.41	92.80	0.09	0.12	
6hr, 1280C, 4% O2	0.03531	7785100	274891.881	2791.17	98.49	0.10		
	0.06607	7785100	514361.557	2809.5	183.08	0.18		
	0.06024	7785100	468974.424	2805.2	167.18	0.17	0.15	
1.5h, 1280C, 3% O2	0.05675	7785100	441804.425	2794.86	158.08	0.16		
	0.13295	7785100	1035029.045	2796.24	370.15	0.37		
	0.07402	7785100	576253.102	2861.93	201.35	0.20	0.24	
1.5h, 1280C, 4% O2	0.17341	7785100	1350014.191	2791.28	483.65	0.48		
	0.0808	7785100	629036.08	2797.1	224.89	0.22		
	0.12741	7785100	991899.591	2794.54	354.94	0.35	0.35	
3hr, 1280C, 3% O2	0.12205	7785100	950171.455	2788.19	340.78	0.34		
	0.08948	7785100	696610.748	2790.53	249.63	0.25	0.30	
3hr, 1280C, 4% O2	0.06995	7785100	544567.745	2786.71	195.42	0.20		
	0.07551	7785100	587852.901	2848.11	206.40	0.21		
	0.06299	7785100	490383.449	2842.34	172.53	0.17	0.19	
3hr, 1210C, 3% O2	0.06699	7785100	521523.849	2794.05	186.66	0.19		
	0.04555	7785100	354611.305	2941.51	120.55	0.12		
	0.03505	7785100	272867.755	2818.68	96.81	0.10	0.13	

APPENDIX

3hr, 1210C, 4% O2	0.05991	7785100	466405.341	2805.26	166.26	0.17		
	0.04791	7785100	372984.141	2805.67	132.94	0.13		
	0.05222	7785100	406537.922	3014.17	134.88	0.13	0.14	
conditions	scale fraction	frame area	scale area	scale width (um)	residual thickness (um)	residual thickness (mm)	averages (mm)	
6hr, 1210C, 3% O2	0.05778	7785100	449823.078	2793.29	161.04	0.16		
	0.04154	7785100	323393.054	2790.21	115.90	0.12		
	0.03543	7785100	275826.093	2815.77	97.96	0.10	0.12	
6hr, 1210C, 4% O2	0.11114	6.97E+06	774224.5794	2682.21	288.65	0.29		
	0.25889	7785100	2015484.539	2824.8	713.50	0.71		
	0.08273	7785100	644061.323	2854.65	225.62	0.23	0.41	
1.5h, 1210C, 3% O2	0.03623	7785100	282054.173	2790.47	101.08	0.10		
	0.04674	7785100	363875.574	2883.66	126.19	0.13		
	0.0333	7785100	259243.83	2865.91	90.46	0.09	0.11	
1.5h, 1210C, 4% O2	0.03531	7785100	274891.881	2781.87	98.82	0.10		
	0.03049	7785100	237367.699	2891.54	82.09	0.08		
	0.02951	1.80E+07	532056.447	4248.78	125.23	0.13	0.10	
304								
6hr, 1280C, 3% O2	0.14949	7785100	1163794.599	2792.52	416.75	0.42		
	0.10319	7785100	803344.469	2803.2	286.58	0.29		
	0.15297	7785100	1190886.747	2589.54	459.88	0.46	0.39	
6hr, 1280C, 4% O2	0.13591	7785100	1058072.941	2796.59	378.34	0.38		
	0.07599	7785100	591589.749	2838.95	208.38	0.21		
	0.0797	7785100	620472.47	2794.26	222.05	0.22	0.27	

APPENDIX

1.5h, 1280C, 3% O2	0.12798	7785100	996337.098	2743.67	363.14	0.36		
	0.08433	7785100	656517.483	2801.82	234.32	0.23		
	0.06574	7785100	511792.474	2736.21	187.04	0.19	0.26	
1.5h, 1280C, 4% O2	0.22375	7785100	1741916.125	2780.7	626.43	0.63		
	0.12483	7785100	971814.033	2792.3	348.03	0.35		
	0.09052	7785100	704707.252	2915.94	241.67	0.24	0.41	
					residual	residual		
conditions	scale fraction	frame area	scale area	scale width (um)	thickness (um)	thickness (mm)	averages (mm)	
3hr, 1280C, 4% O2	0.15609	7785100	1215176.259	2790.18	435.52	0.44		
	0.15794	7785100	1229578.694	2797.7	439.50	0.44		
	0.13439	7785100	1046239.589	2802.49	373.33	0.37	0.42	
3hr, 1280C, 3% O2	0.22525	7785100	1753593.775	2795.49	627.29	0.63		
	0.19309	7785100	1503224.959	2810.17	534.92	0.53	0.58	
3hr, 1250C, 4% O2	0.04765	7785100	370960.015	2793.41	132.80	0.13		
	0.08311	7785100	647019.661	2835.55	228.18	0.23		
	0.07546	7785100	587463.646	2888.69	203.37	0.20	0.19	
6hr, 1250C, 4% O2	0.07311	7785100	569168.661	2833.82	200.85	0.20		
	0.04901	7785100	381547.751	2790.39	136.74	0.14		
	0.08098	7785100	630437.398	2851.98	221.05	0.22	0.19	
3hr, 1250C, 3% O2	0.10119	7785100	787774.269	2780.2	283.35	0.28		
	0.12208	7785100	950405.008	2798.56	339.61	0.34		
	0.10739	7785100	836041.889	2813.84	297.12	0.30	0.31	

1.5hr, 1250C, 3% O2	0.20583	7785100	1602407.133	2796.15	573.08	0.57		
	0.09931	7785100	773138.281	2794.9	276.62	0.28	0.42	
6hr, 1250C, 3% O2	0.11368	7785100	885010.168	2780.05	318.34	0.32		
	0.11485	7785100	894118.735	2832.39	315.68	0.32		
	0.07389	7785100	575241.039	2798.56	205.55	0.21	0.28	
1.5h, 1250C, 4% O2	0.30795	7785100	2397421.545	2799.92	856.25	0.86		
	0.11883	7785100	925103.433	2795.79	330.89	0.33		
	0.12106	7785100	942464.206	2798.19	336.81	0.34	0.51	

APPENDIX

APPENDIX 7

SCANNING ELECTRON MICROGRAPHS OF SOME OF REMAINING RESULTS

The figure below shows the appearance of the exterior surface of a descaled type 304 sample, showing that the appearance of the cracked residual scale reflects the underlying austenite grain structure.

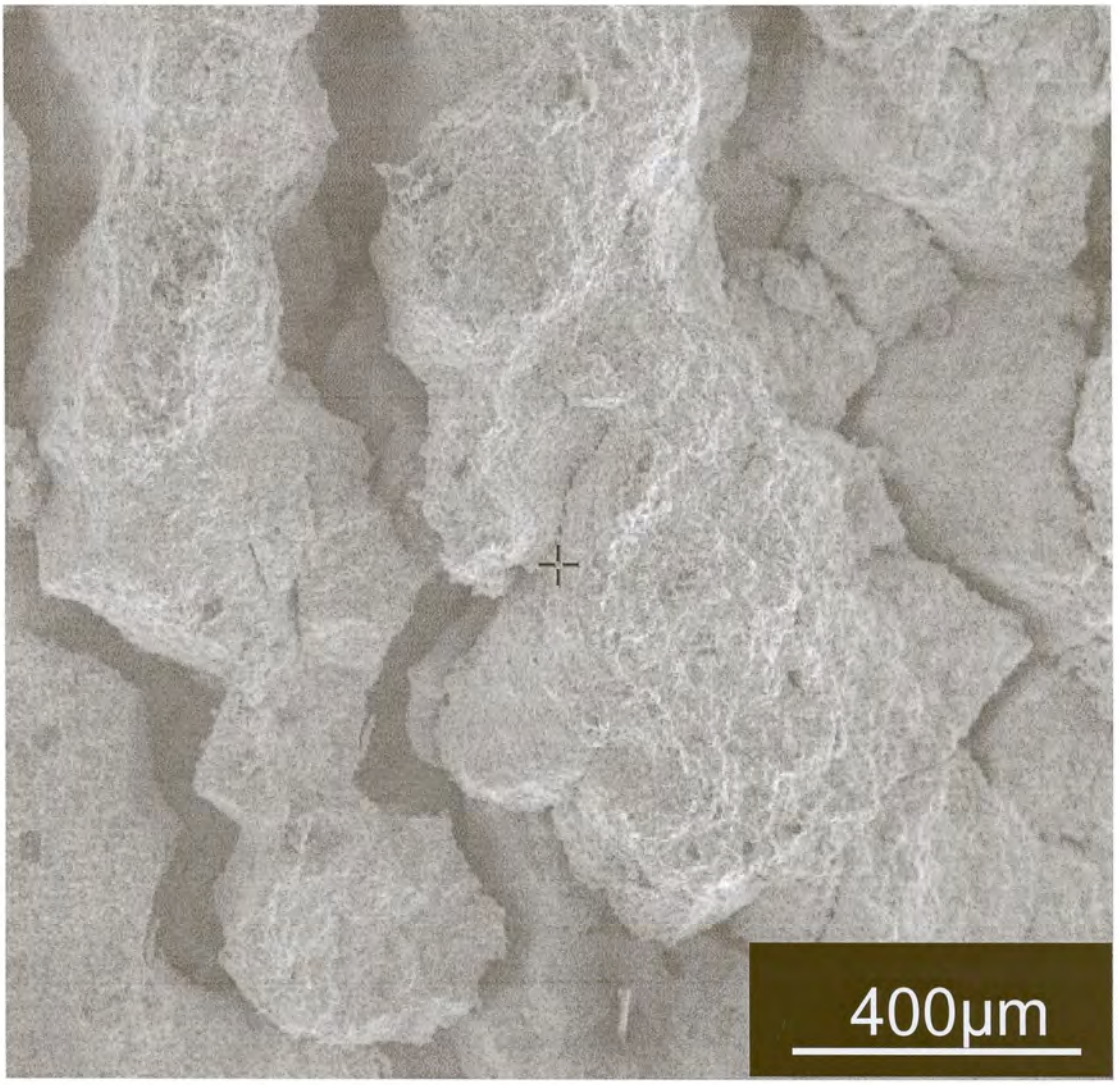

The topography visible in this image is that of the residual scale attached to a type 412 stainless steel sample.

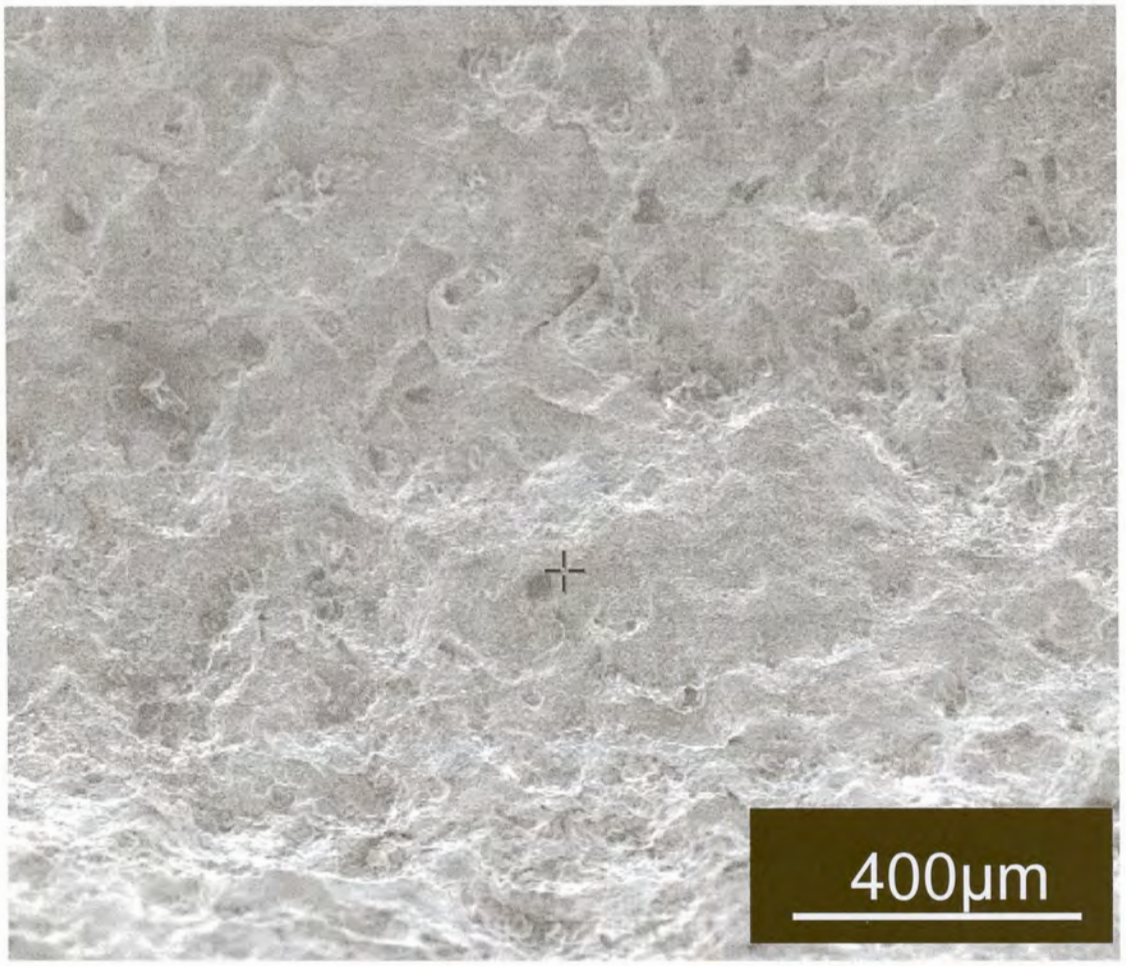

Montage of descaled surface of type 304 sample, showing that the residual scale thickness corresponds to the full thickness of the entangled region. The scale is towards the upper part of the image and the steel substrate towards the bottom. This sample was oxidized at a reheating temperature of 1250 ^{0}C, with 4% excess oxygen for 3 hours.

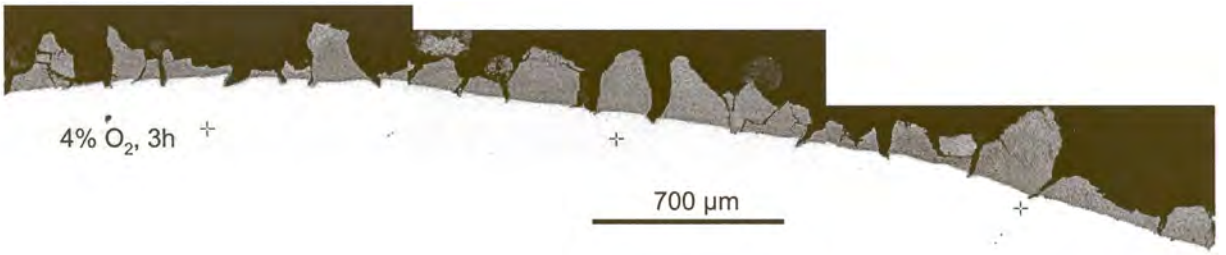

Montage of descaled surface of type 412 stainless steel sample. This sample was oxidised at a reheating temperature of 1210 ^{0}C, with 3% excess oxygen for 6 hours.

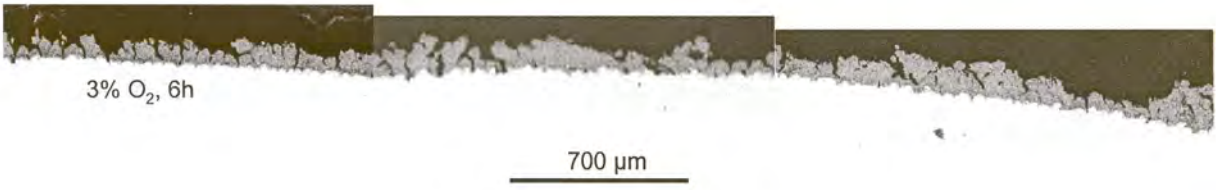

Etched cross-sections of type 304 samples reheated at 1250 ^{0}C. Samples were electrolytically etched in oxalic acid to reveal microstructure of the steel. Cracks in the residual steel can be seen to correspond to grain boundaries in the underlying microstructure.